

Article

# A Lightweight Structure Redesign Method Based on Selective Laser Melting

Li Tang, Chunbing Wu \*, Zhixiong Zhang, Jianzhong Shang and Chao Yan

College of Mechatronics and Automation, National University of Defense Technology, Changsha 410073, China; tangli@nudt.edu.cn (L.T.); zzxnudt2010@sina.com (Z.Z.); jz\_shang\_nudt@163.com (J.S.); mech\_yan@foxmail.com (C.Y.)

\* Correspondence: wuchunbing14@nudt.edu.cn; Tel.: +86-155-7086-4869

Academic Editor: Manoj Gupta

Received: 10 September 2016; Accepted: 1 November 2016; Published: 16 November 2016

**Abstract:** The purpose of this paper is to present a new design method of lightweight parts fabricated by selective laser melting (SLM) based on the “Skin-Frame” and to explore the influence of fabrication defects on SLM parts with different sizes. Some standard lattice parts were designed according to the Chinese GB/T 1452-2005 standard and manufactured by SLM. Then these samples were tested in an MTS Insight 30 compression testing machine to study the trends of the yield process with different structure sizes. A set of standard cylinder samples were also designed according to the Chinese GB/T 228-2010 standard. These samples, which were made of iron-nickel alloy (IN718), were also processed by SLM, and then tested in the universal material testing machine INSTRON 1346 to obtain their tensile strength. Furthermore, a lightweight redesigned method was researched. Then some common parts such as a stopper and connecting plate were redesigned using this method. These redesigned parts were fabricated and some application tests have already been performed. The compression testing results show that when the minimum structure size is larger than 1.5 mm, the mechanical characteristics will hardly be affected by process defects. The cylinder parts were fractured by the universal material testing machine at about 1069.6 MPa. These redesigned parts worked well in application tests, with both the weight and fabrication time of these parts reduced more than 20%.

**Keywords:** 3D printing; selective laser melting (SLM); part redesign; SLM structure performance; frame structure reconstruction

## 1. Introduction

There is an increasing demand for lightweight parts in the aerospace, automotive, medical industries and other fields with good mechanical characteristics and shorter manufacturing times. However, there are often redundant materials in conventional parts because of the conventional manufacturing processes' inherent restrictions, which make it difficult to get a lightweight component.

Selective laser melting (SLM) is an additive manufacturing (AM) process which can directly make complex three-dimensional metal parts according to Computer Aided Design (CAD) data by selectively melting successive layers of metal powders [1]. It is an alternative to conventional manufacturing processes [2,3]. The tool-less fabrication and geometric freedom offered by SLM show great potential to make advanced lightweight structures and products which are highly desired by engineering sectors. It permits new design methods for lightweight structures that were not possible before because of the limitations of conventional manufacturing processes.

Currently, there are some approaches for lightweight parts design with the use of SLM. Among all of the methods, the design of cellular structures and structure topological optimization are very common.

The cellular structure design method replaces the interior structures of the parts with cellular structures which have relatively less mass than solid material. Cellular structures can be classified into two categories: stochastic porous structures and periodic cellular lattice structures according to the distribution of the internal micro-structure. Stochastic porous structures are filled with open or closed voids that distribute randomly, whereas periodic cellular lattice structures consist of repeating unit cells leading to a uniform structure. Because of the uneven distribution of materials, periodic lattice structures show finer mechanical characteristics than stochastic porous structures when they have the same volume fraction [4,5]. A few previous works have been done to study the manufacturing of lightweight cellular structures with the use of SLM. Campanelli et al. [6] investigated a lattice structure comprised of four vertical strut columns and four pairs of struts. This structure was made by SLM using titanium alloy Ti6Al4V. A campaign was planned to compare the behavior of the lattice structure with variable cells, truss sizes and vertical bars as reinforcements. They used Taguchi's method to minimize the number of experiments. Compression tests were performed to study the mechanical behavior of the lattice structures. They demonstrated that when the cell size is smaller, and the size of the strut edge and the relative density are the highest, this structure shows the highest strength. Wang et al. [7] investigated the design rules and the key points to fabricate porous structures. Thin walls, cylinders with different geometrical dimensions and overhanging structures with different inclined angles were designed and fabricated to obtain the SLM fabricating resolution and the critical inclined angle for designing the porous structures. The experiments for fabricating porous structures with different sizes were also conducted. The results showed that the porous structure can be well fabricated by SLM.

Hernandez et al. [8] researched the micro-structure and dimensional accuracy of the as-manufactured lattices with the same morphology with the exception of the strut diameter, which was varied systematically. They found that the variation in the compressive yield stress with the strut diameter is in good accordance with simple models based on compressive deformation rather than shearing or buckling. Besides, struts normal to the build direction showed more significant defects. To examine the effect of cellular lattice structures on the strength of parts, Mahshid et al. [9] analyzed the collapse strength of lattice structures by finite element (FE) and mathematical models. Compression tests of the solid, hollow, non-rotated-closed-cellular and rotated-closed-cellular samples were performed. The results showed that the cellular structures heavily influence the compression strength and showed only an increase of 11.4% at the highest point with respect to hollow specimens.

Sing et al. [10] investigated the dimensional accuracy and compressive behavior of cellular lattice structures with different unit cell types, namely the square pyramid, truncated cube and octahedron unit cells. Analysis of variance (ANOVA) was also carried out to determine the significance of various process and design parameters on the dimensional accuracy and compressive strength of the lattice structures. They found that the processing parameters, such as laser power and laser scan speed, have no significant effect on the elastic constant but have a significant effect on the powder adhesion on the struts, affecting the dimensional accuracy. However, geometrical design parameters such as the unit cell type and strut diameter have significant effects on the elastic constant but not on the dimensional accuracy of the lattice structures.

These previous works showed that the manufacturability of cellular lattice structures was often affected by the lattice unit size. Besides, the mechanical characteristics of lattice micro-structures are always affected by manufacturing defects, especially when the unit size is very small.

Another common method of lightweighting is the use of structure topological optimization. This design method generates an optimized material distribution for particular purposes by minimizing a suitable objective within the limited space. Some previous works have investigated this method to take advantage of the SLM process. Brandt et al. [11] studied the design, manufacture and examination of high-value aerospace components and investigated the geometric optimization of the aerospace bracket from Ti-6Al-4V alloy. Xiao et al. [12] examined the design and fabrication of bio-material scaffolds using topological optimization with the SLM process. An optimization

procedure was proposed to seek a micro-structure of maximum stiffness with the constraint of volume fraction optimization. The inverse homogenization theory was also applied to estimating the effective mechanical properties of scaffold materials which are arrayed by periodical base cells.

However, the structure topological optimization will always change the shape of the components. The shape of parts should not change, especially when the parts are assembled with other traditional components or should meet the requirements of aerodynamics.

This paper investigates a new design method for lightweight parts manufactured by selective laser melting (SLM) based on the “Skin-Frame” and explores the influence of machining defects on SLM parts which have different sizes by the experimental method. The procedures of the novel, lightweight redesign method were researched. A stopper and connecting plate were redesigned with this method. These redesigned parts were fabricated by SLM and showed good mechanical characteristics. The results show that the lightweight parts designed by this method can satisfy the use requirements.

## 2. Experimental Section

### 2.1. Materials

The lattice structures and tensile test samples were made from an iron-nickel alloy (IN718) powder with an average particle size of  $30 \pm 10 \mu\text{m}$ . The chemical composition of the powder consists of Ni (53.5%), Cr (19%), Fe (18.3%), Nb (5%), Mo (3% max), Ti (1% max), Al (0.43% max). The SEM micro-graph of the IN718 powder is shown in Figure 1. It has good mechanical characteristics and is widely used in aerospace industry. All samples for this study were manufactured by EOSINT M280 system which utilized a 200 W ytterbium fiber laser. This machine has an effective building volume of  $250 \text{ mm} \times 250 \text{ mm} \times 325 \text{ mm}$ . Tensile candidates were fabricated in a vertical build orientation, with the cylinder axis parallel to the beam direction.

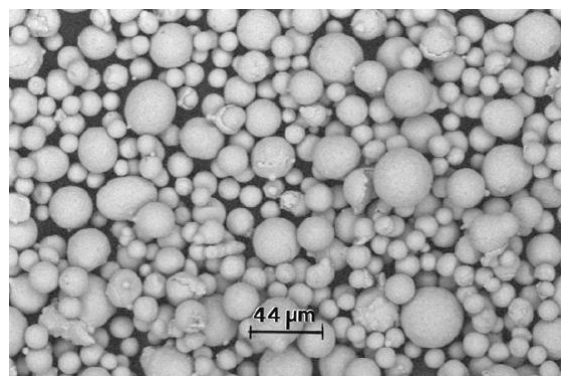
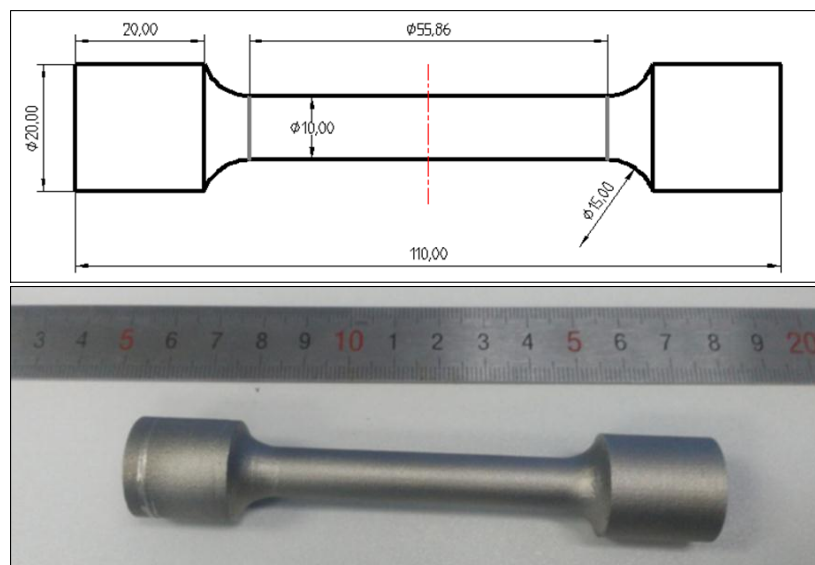


Figure 1. SEM micro-graph of the IN718 powder.

The  $100 \mu\text{m}$  diameter laser beam was scanned at  $1200 \text{ mm/s}$  in argon gas environments surrounding the building parts. The oxygen level in the process chamber was maintained below 0.1%. The building platform was preheated to  $80 \text{ }^\circ\text{C}$  and maintained at that temperature. The hatch spacing was  $0.05 \text{ mm}$  and the layer thickness was  $50 \mu\text{m}$  with a spot diameter of  $0.1 \text{ mm}$ .

### 2.2. Process of Tensile Test

Tensile samples were designed according to the Chinese GB/T 228-2010 standard. Figure 2 shows the sizes of samples for the tensile experiment. The diameter of parts is  $10 \text{ mm}$  while the rest of the parameters depend on the test machine. The samples were designed by CAD software then exported as a single STL file format to the SLM machine for manufacturing.



**Figure 2.** Dimensions of the tensile test sample.

The experiments were performed in the universal material testing machine INSTRON 1346 (Instron, Norwood, MA, USA) at room temperature with a loading speed of  $0.008 \text{ mm}\cdot\text{s}^{-1}$ . The strain rate is approximately  $1 \times 10^{-3} \text{ s}^{-1}$ . The maximum load of this machine is 2000 KN with a loading accuracy of  $\pm 5\%$ . The samples were clamped on the machine and the load was gradually increased until the samples were fractured to get their tensile curve. The tensile strength and other properties can be calculated by Equation (1) and the tensile curve:

$$\sigma = \frac{P}{S} \quad (1)$$

where  $\sigma$  is the section stress,  $P$  and  $S$  are the maximum load and section area, respectively.

$$\varepsilon = \frac{L - L_0}{L_0} \quad (2)$$

The elongation percentage  $\varepsilon$  can be calculated by initial length  $L_0$  and fracture length  $L$ .

### 2.3. Compression Test of Lattice Structure

Compression test candidates were designed according to the Chinese GB/T 1452-2005 standard. The compression samples have the sandwich construction with 16 cylinder units in the middle. The height of a cylinder unit is 15 mm and the thickness of the panels is 1 mm with a parallelism tolerance of 0.1 mm.

Because of the thermal stress brought by the temperature difference during the SLM process, the warping deformation of thin-walled parts such as the panel will always occur as shown in Figure 3a. The deformation will have an impact on the dimensional accuracy and structural properties of the parts. So the samples were produced by the SLM process with additional skin on the vertical direction to avoid large deformation and get a higher parallelism tolerance as shown in Figure 3b. The additional skin was cut by wire-electrode cutting as shown in Figure 3c.

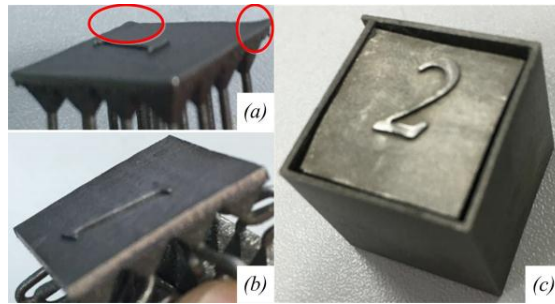


**Figure 3.** Large curling of direct manufacturing candidate (a), small curling of sample fabricated with additional skin after wire-electrode cutting (b) and sample fabricated with additional skin (c).

The diameters of the cylinders are 0.5 mm, 1.0 mm, 1.5 mm, 2.0 mm, 2.5 mm, respectively, as shown in Figure 4. The compression tests were performed in the MTS Insight 30 compression testing machine (MTS, Minneapolis, MN, USA) at room temperature with a loading speed of  $0.05 \text{ mm s}^{-1}$ . The control strategy is Posn. The samples were tested in a constant loading speed in this strategy. The maximum load of this machine is 30 KN with a loading accuracy of  $\pm 5\%$ . This experiment was by recorded by a camera to help to study the trends of yield process of different structure sizes.



**Figure 4.** Compression test samples with different parameters.

### 3. Lightweight Parts Redesign Method

This method disassembled parts by its shape and force condition and reconstructed the inner structure of each divided one by corresponding the framework structure which was optimized by the finite element method, and then mixed them together with the main framework. Optimized foundation frameworks can be reserved to build the framework library, which can greatly shorten the design time using this method. The basic flow of this approach is shown in Figure 5.

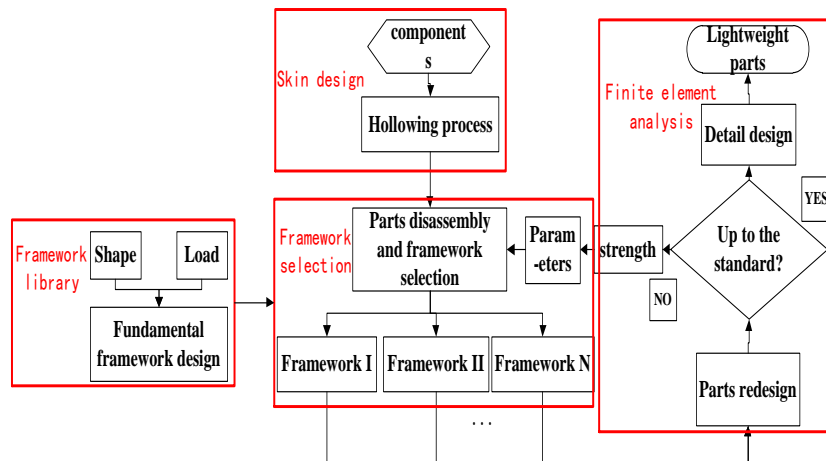


**Figure 5.** Flow chart of lightweight redesign method.

The main steps include three aspects as follows:

1. Design of the skin

A suitable skin thickness of the components is necessary to maintain the shape of parts. This paper studied the strain and stress of parts with different skin thicknesses and loads.

2. Parts disassembly and framework design

The components were disassembled by their shape and force conditions. Different optimized frameworks were selected from the framework library or were newly designed to fill the disassembled parts. These newly designed frameworks can be reserved at the framework library by their shape and load. Use of the framework library can greatly shorten the design period compared with topology optimization of the whole part. The design of new parts can be as easy as selecting fundamental frameworks to fill the parts.

3. Finite element analysis and details of parts

We assembled the divided parts together by their topology structure and study the characteristics of components using the finite element method. Improve the details such as the metal outlet position of the metal powder according to the SLM process.

### 3.1. Design of Skin

The quality of thin-wall parts manufactured by the SLM process will be affected by their thickness. The thicker the thin-wall parts are, the better the quality will be. However, thick walls will bring about a higher weight of the components, which makes it difficult to get lightweight parts. The optimum thickness of the skin was studied by the finite element analysis of an empty cube with different loads and wall thicknesses as shown in Figure 6.

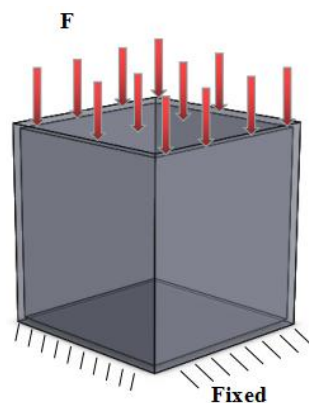


**Figure 6.** Model of thin-wall parts for finite element analysis.

The side length of the cube is 100 mm. The bottom side was fixed and uniform loads of 500 N and 1000 N were applied, respectively, to the top side to test the mechanical performance of different thin walls under various loads. The results of the finite element analysis are reported in Table 1 and Figures 7 and 8.

**Table 1.** Analysis result of thin-wall parts with different thicknesses and loads.

Thickness (mm)	Load (N)	Maximum Stress (MPa)	Maximum Strain (mm)	Weight (g)
0.5	500	112.4	0.73937	238
	1000	290.75	2.028	
1	500	68.054	0.37832	470
	1000	148.36	0.75461	
1.5	500	35.469	0.13709	699
	1000	70.939	0.27418	

Table 1. Cont.

Thickness (mm)	Load (N)	Maximum Stress (MPa)	Maximum Strain (mm)	Weight (g)
2	500	14.705	0.039352	922
	1000	29.411	0.078705	
2.5	500	10.02	0.020339	1141
	1000	18.385	0.043148	

It is shown in Figures 7 and 8 that the maximum stress and strain decrease with the increase of the thickness of the skin. The decrease trend becomes gentle when the thickness of the skin is greater than 2 mm. These results allow us to conclude that the most suitable thickness of the skin is 2 mm to obtain a lightweight component produced by the SLM process.

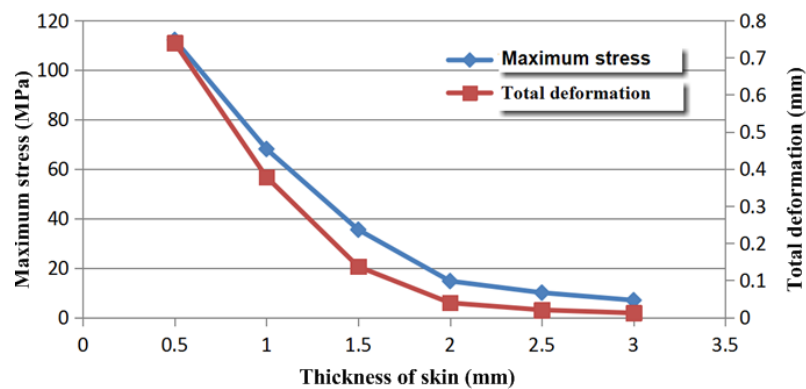


Figure 7. Stress and strain of skin under load of 500 N.

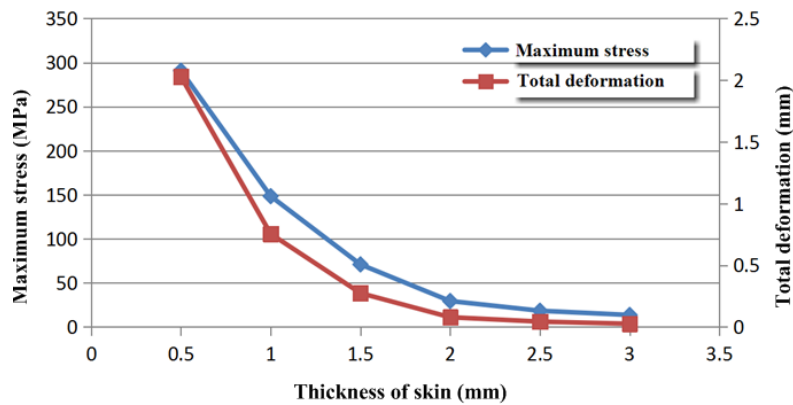
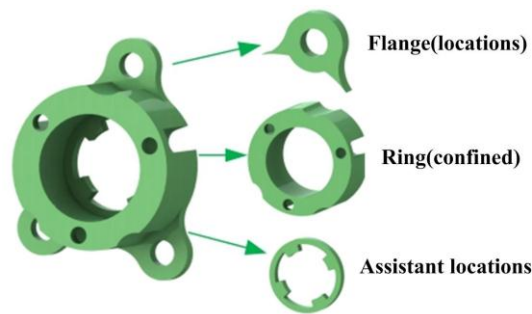


Figure 8. Stress and strain of skin under load of 1000 N.

### 3.2. Parts Disassembly and Framework Design

The parts can be divided by their force conditions such as the bending moment, torque, tensile, compression, shearing force or a possible combination of them. The shapes of the components also need to be considered. The elementary shapes of the structure include: cuboid, cylinder, ring, sphere, L shape and so on.

Finally, the auxiliary functions of each part should be taken into account. The common assistant functions include: bolt mounting hole, key-way, locations and so on. The parts were disassembled as shown in Figure 9. Each divided one should be redesigned for a lighter structure after the disassembly. The topological optimization of frameworks design was performed using Optistruct software (Altair, Troy, NY, USA). Some typical structures were redesigned as follows.



**Figure 9.** An example of parts disassembly.

### 3.2.1. Flange Frame with Torque

The flange often bears the torsional moment from its bolt holes. According to the following conditions, the optimal design of the framework of the structure was carried out.

- (1) Objective function: minimum structure mass
- (2) Condition: flange bears torsion load
- (3) Boundary conditions: the bolt holes are fixed and the inner surface of the flange is applied to the torque
- (4) Design space: brown region in graph
- (5) Minimum thickness: 0.006 m
- (6) Design constraints: meeting the strength requirements with minimum mass

According to the topology optimization conditions above, the original part model was defined as shown in Figure 10a. The framework obtained by topology optimization can be seen in Figure 10b. This new structure was taken into ANSYS Workbench to analyze its strength. The stress distribution on the structure became uniform after optimization, as shown in Figure 10c.

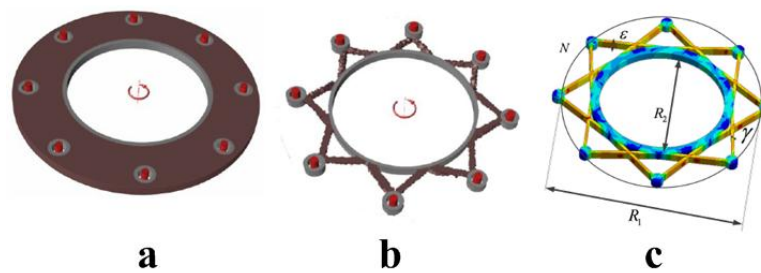


**Figure 10.** The original flange model (a), flange framework obtained by topology optimization (b), stress distribution of flange frame (c).

The comparison of the stress distribution density before and after optimization is shown in Figure 11. As can be seen from Figure 11, the two structures have the same maximum stress and the average stress of the optimized structure became larger. Thus, the utilization ratio of the structure was improved.

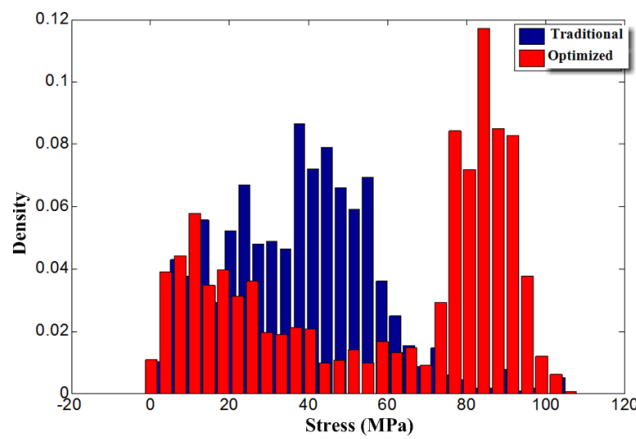


Figure 11. Stress distribution density of traditional and optimized flange.

The main parameters of the flange frame are:

- $N$ : number of mounting holes;
- $D_1$ : location diameter of mounting holes;
- $D_2$ : diameter of inner ring;
- $\epsilon$ : thickness of flange;
- $\zeta$ : ratio of outer and inner ring;
- $\gamma$ : thickness of dowel bar;
- $\mu$ : equivalent stress;
- $M$ : applied torque;
- $\sigma_s$ : yield strength of material

The equivalent stress  $\mu$  can be calculated by following formulas:

$$\mu = \frac{\sigma_s}{MD_2\epsilon} \tag{3}$$

$$\zeta = \frac{D_1}{D_2} \tag{4}$$

The thickness of the dowel bar  $\gamma$  is variable to get parts with different performances. The structures with different parameters were analyzed by ANSYS Workbench. The analysis results of structures with constant  $\zeta = 1.6$  and  $N = 12$ , respectively, are shown in Figure 12.

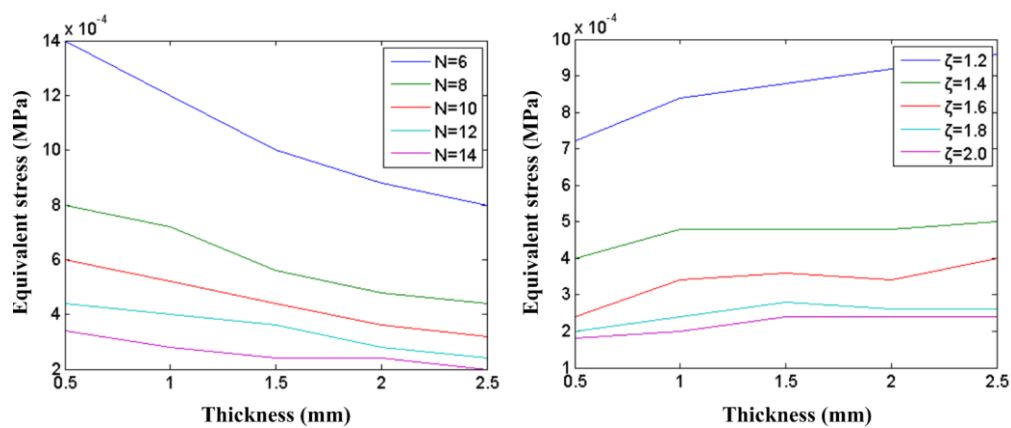


Figure 12. Influence of design parameters on the structural stress of the flange.

### 3.2.2. Rectangular Frame with Bending Moment

The cuboid applied bending moment was analyzed in this section. According to the following conditions, the optimal design of the framework was carried out.

- (1) Objective function: minimum structure mass
- (2) Condition: cuboid bearing bending load
- (3) Boundary conditions: the left surface is fixed and the right surface is applied to the surface force
- (4) Design space: brown region in graph
- (5) Minimum thickness: 0.006 m
- (6) Design constraints: meeting the strength requirements with minimum mass

According to the topology optimization conditions above, the original part model was defined as shown in Figure 13a. The topology optimization method was used to get the framework shown in Figure 13b. The final structure after optimization can be seen in Figure 13c. The thickness of frame  $\eta$  was taken as a design parameter to get parts with different performances.

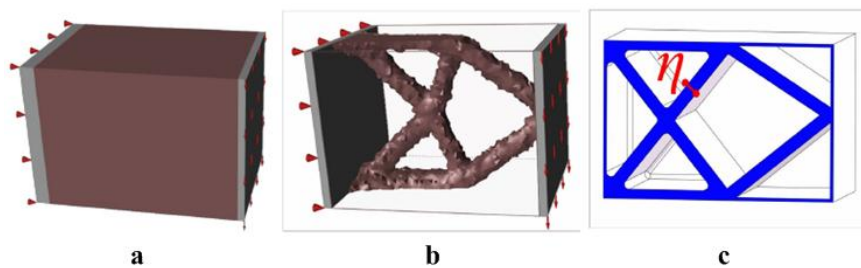


**Figure 13.** The original cuboid model (a), rectangular frame obtained by topology optimization (b), the final rectangular frame after optimization (c).

### 3.2.3. Ring Frame with Torque

The bidirectional torsional moment was applied to the ring. The optimal conditions were set as follows.

- (1) Objective function: minimum structure mass
- (2) Condition: inner race bearing torsion load
- (3) Boundary conditions: the outer ring is fixed and the inner race is applied to torque
- (4) Design space: brown region in graph
- (5) Minimum thickness: 0.006 m
- (6) Design constraints: meeting the strength requirements with minimum mass

The traditional part model is shown in Figure 14a. The preliminary framework can be obtained by the topology optimization method as shown in Figure 14b. The final part structure after optimization can be seen in Figure 14c.

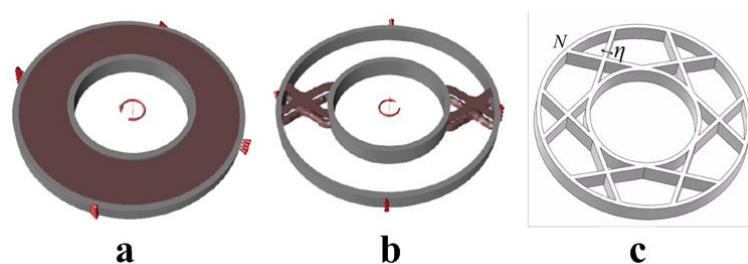


**Figure 14.** The original ring model (a), ring frame obtained by topology optimization (b), the final ring frame after optimization (c).

The comparison between the stress distribution density of the traditional (Figure 14a) and optimized parts (Figure 14c) is shown in Figure 15. As can be seen from Figure 15, the average stress of the optimized structure became larger. Thus, the efficiency of the structure was improved.

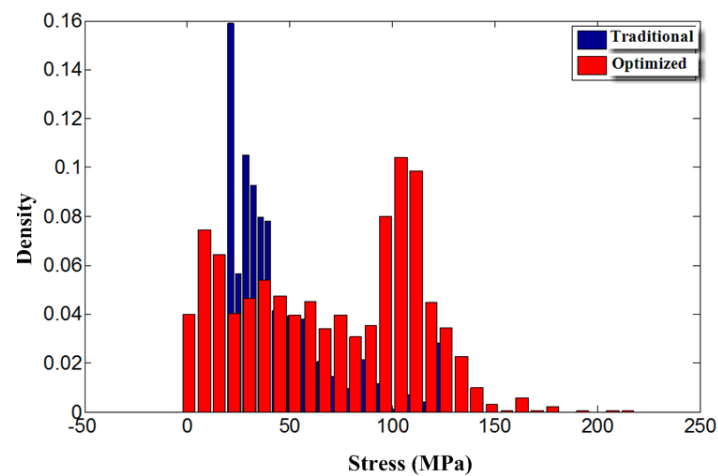


Figure 15. Stress distribution density of traditional and optimized rings.

To get components with different performances, the number of stiffeners  $N$  and the thickness of the frame  $\eta$  were taken as design parameters. Figure 16 shows the finite element analysis results which illustrate the influence of the number of stiffeners  $N$  and the thickness of frame  $\eta$  on the structure stress. The performance of the structure improved with these two parameters.

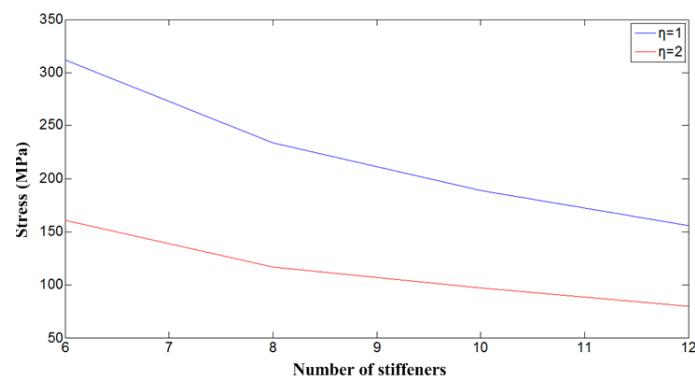


Figure 16. Influence of design parameters on the structural stress of ring.

### 3.2.4. L-Shape Frame with Bending Moment

The L-shape structure often bears the bending moment. The optimization conditions are defined as follows.

- (1) Objective function: minimum structure mass
- (2) Condition 1: one end is fixed and the other end is applied to the vertical load;
- (3) Condition 2: one end is fixed and the other end is applied to the horizontal load
- (4) Boundary condition: the right boundary is fixed and the left surface is applied to the surface force
- (5) Design space: brown region in graph
- (6) Minimum thickness: 0.006 m
- (7) Design constraints: meeting the strength requirements with minimum mass

According to the topology optimization conditions above, the original part model was defined as shown in Figure 17a. The topology optimization method was used to get the framework shown in Figure 17b. The final structure after optimization can be seen in Figure 17c. The thickness of frame  $\eta$  was taken as a design parameter.

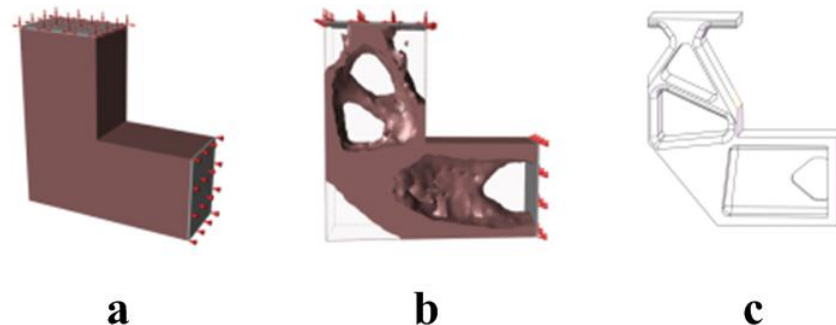


**Figure 17.** The original L-shape model (a), L-shape frame obtained by topology optimization (b), the final L-shape frame after optimization (c).

### 3.3. Detail Design

There are some detailed structures such as the fillet, chamfer, keyway, gear teeth, splines, mounting hole and so on which are important when the parts cooperate with other components. To ensure the functions of these structures, they should not be redesigned.

After the reconstruction of the structures, stress concentration may occur because of the sharp change of the cross-section area caused by the intersecting frame. In order to improve the parts' performance, the fillets of the frames need to be considered, which can help to reduce the local stress concentration.

There are still some powders in the closed holes of the redesigned parts manufactured by the SLM process which will increase the weight and cost of the components. Thus, powder outlets should be considered to discharge powders smoothly. The fillets and powder outlets are shown in Figure 18.

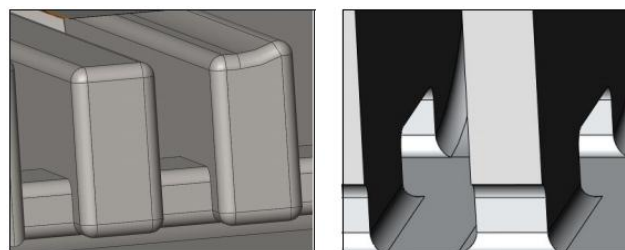


**Figure 18.** The fillets and powder outlets of SLM parts.

### 3.4. Application

#### 3.4.1. Case 1: Stopper

The stopper was used in an automatic device to avoid the forward movement of this device. The actual installation and use conditions of this part are shown in Figure 19.

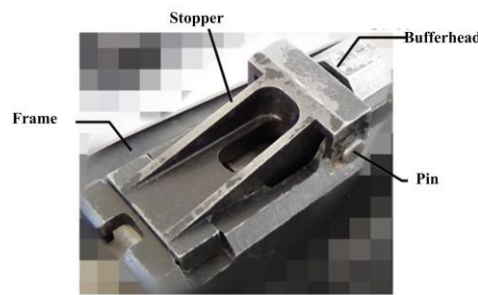


Figure 19. The use conditions of stopper.

According to the design method researched before, the redesign processes of the stopper are shown as follows.

1. Model building and design of the skin

The model can be made by 3D scanning and reverse engineering technology. The optimized thickness of the skin is 2 mm according to the previous work.

2. Stopper structure severing and framework design

The stopper can be divided into four parts by their force conditions and shapes: the L-shape structure with bending moment, the rectangular structure one with bending moment, the rectangular structure two with bending moments, and the thin-wall structure. The framework of each divided part was redesigned by the method studied in Section 3. Then the redesigned stopper was connected by their topological relationship. The reconstruction result is shown in Table 2.

Table 2. Disassembly of stopper.

Number	Design Objects	Shape	Load	Design Parameters	Result
0			Skin	Thickness of skin $\beta$	
1		L shape	Bending moment	Thickness of frame $\lambda$	
2		Rectangular	Pressure	Thickness of frame $\eta$ Number of frame $N_1$	
3		Rectangular	Pressure	Thickness of frame $\alpha$ Number of frame $N_2$	
4			Thin-wall structure	$\infty$	

3. Finite element analysis and detail design of the stopper

The original and reconstructed stopper models were introduced into ANSYS Workbench for finite element analysis to show the change of stress distribution. Other detailed designs such as fillets and powder outlets were completed in this stage. The two stoppers have the same maximum stress. In addition, the average stress of the optimized stopper became larger.

A load of 1000 KN was applied to the back surface of the stopper while the boundary conditions were added by its actual conditions. The stress distributions of the stopper with different inner

structures are shown in Figure 20. The stress of the original structure concentrates at a low level, which leads to a waste of material. For the original stopper, the mass is 795.2 g and the maximum stress is 211.52 MPa. The stress distribution level of the redesigned stopper increased to a higher level, which can be seen in Figure 21. The weight of the redesigned stopper decreased to 580.0 g with a weight reduction of about 27%. The maximum stress of the redesigned stopper is only 209.77 MPa.

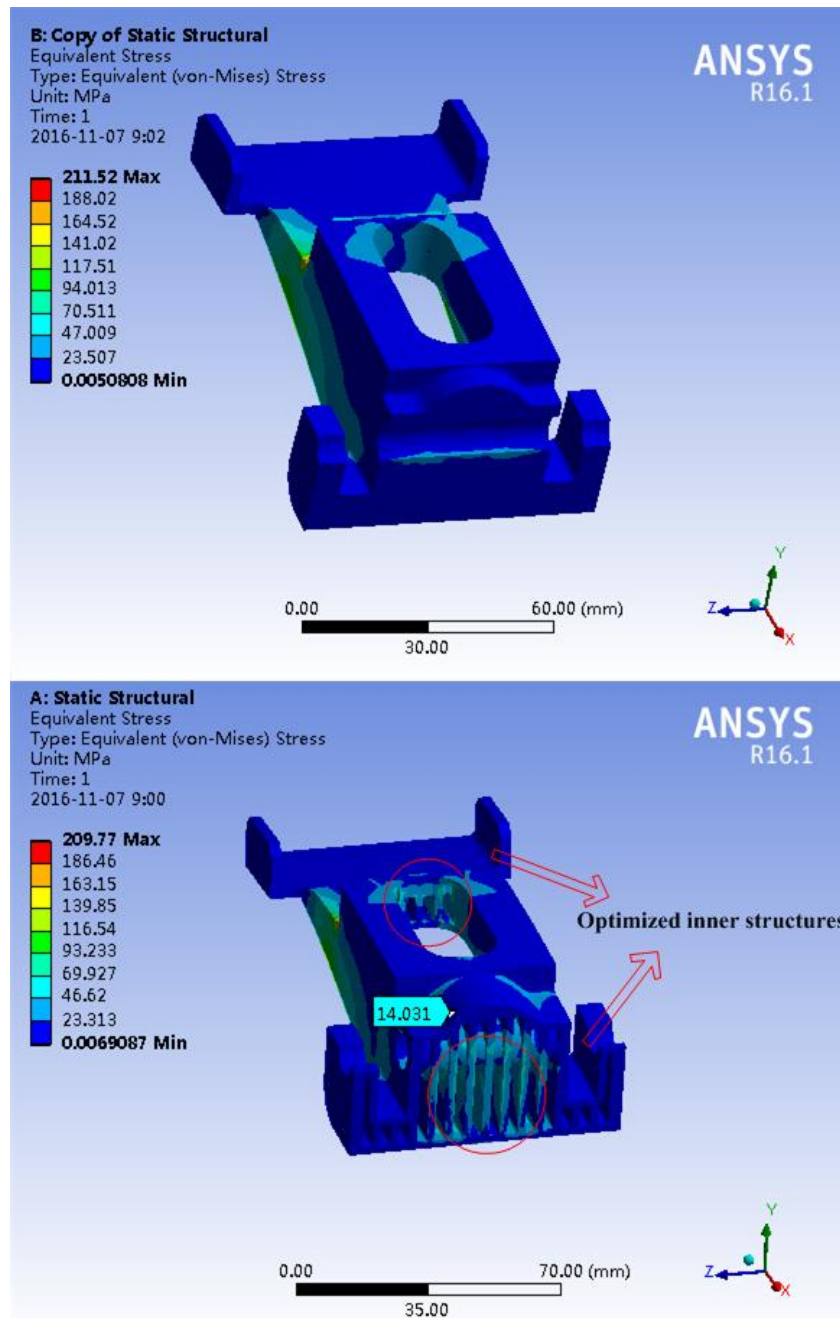
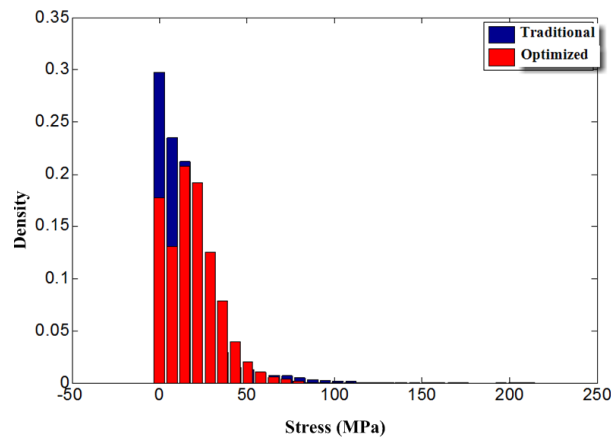


Figure 20. Stress distribution of original (up) and redesigned (down) stopper.



**Figure 21.** Stress distribution density of traditional and optimized stopper.

### 3.4.2. Case 2: Connecting Plate

The connecting plate with inner splines is always used to transfer torque between the main step-down gear and side reducer of a heavy tracked vehicle. It connects with the main reducer by bolts and transfers torque by the splines. The actual use conditions of the connecting plate are shown in Figure 22.

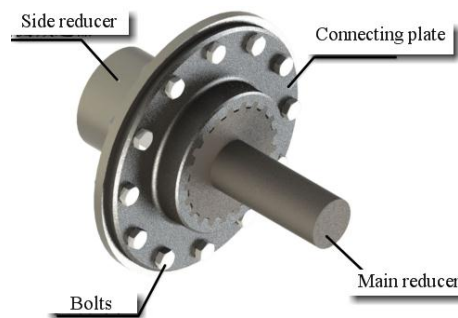


**Figure 22.** The use conditions of the connecting plate.

Similarly, the redesign processes of the connecting plate are as follows.

#### 1. Model building and design of the skin

The model can be made by 3D scanning measuring and reverse engineering technology. The optimized thickness of the skin is 2 mm according to the previous work.

#### 2. Connecting plate structure severing and framework design

The connecting plate can be divided into three parts by their force conditions and shapes: the flange structure with torque, the ring structure with torque and the spline structure. The framework of each divided plate was redesigned by the method studied in Section 3. Then the redesigned connecting plate was connected by their topological relationship. The reconstruction result is shown in Table 3.

#### 3. Finite element analysis and detail design of the connecting plate

The original and reconstructed connecting plate models were introduced into ANSYS Workbench (Pittsburgh, CA, USA) for finite element analysis to show the change of the stress distribution. Other detailed designs such as fillets and powder outlets were completed in this stage.

Table 3. Disassembly of connecting plate.

Number	Design Objects	Shape	Load	Design Parameters	Result
1		Flange	Torque	Thickness of frame $\theta$	
2		Ring	Torque	Thickness of frame $\nu$ Number of frame $N_3$	
3		Spline	Stress	$\infty$	

The boundary conditions were added by its actual conditions. The stress distributions of the original (Figure 23a) and optimized connecting plates (Figure 23c) were compared. The maximum stress of the solid connecting plate is 23.464 MPa in Figure 23a. The maximum stress of the redesigned one is 34.66 MPa, as seen in Figure 23c. At the same time, the maximum deformation of the original connecting plate appeared to be 0.0087 mm in Figure 23b compared with the redesigned one of 0.0064 mm, shown in Figure 23d. The mass of the original connecting plate is 3733.6 g. The weight decreased to 2150.9 g with a weight reduction of about 42.4%. The strength can meet the requirements and the distribution of stress became more uniform.

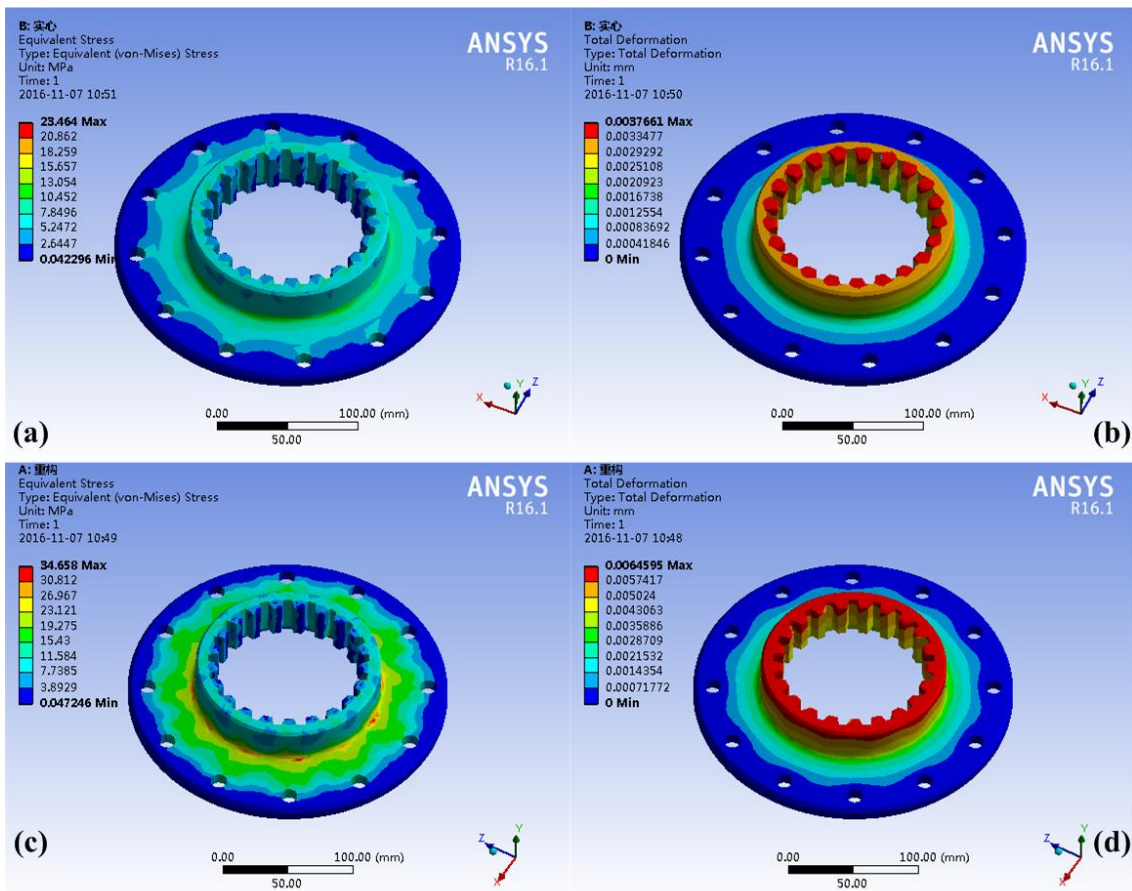
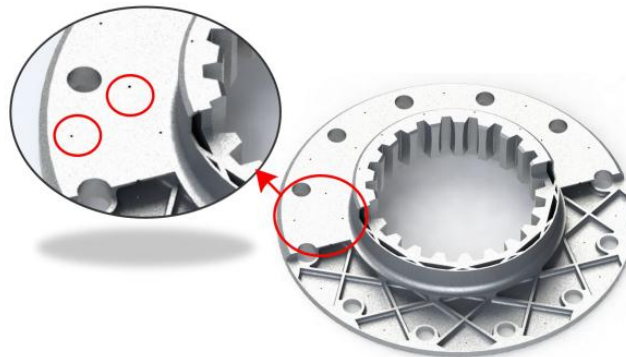


Figure 23. Stress distribution of original connecting plate (a), deformation of original connecting plate (b), stress distribution of redesigned connecting plate (c), deformation of redesigned connecting plate (d).

There are some independent cavities created by the inner frames. Every cavity was given a powder outlet of 1 mm diameter at the appearance of parts to discharge redundant powders. The final design model is shown in Figure 24. The red zone shows the powder outlets of the connecting plate.



**Figure 24.** Final design model of the connecting plate.

The weight of an armored vehicle is 22,500 kg. The redesigned connecting plate was assembled in this vehicle to test its performance in various conditions. The test includes a straight drive test, a pivot turn test, and a brake test at 15 km/h and 30 km/h, respectively. Besides, this vehicle run over 30 km on a gravel road. The assembly procedures are shown in Figure 25.

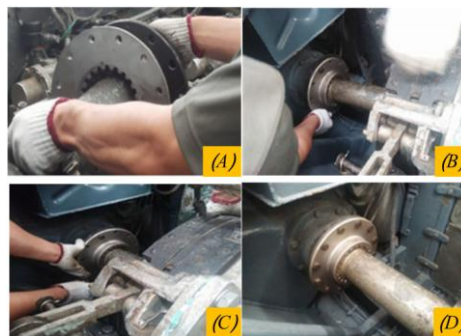


**Figure 25.** The assembly of reduction gear (A), tightening of bolts on connected plate (B), position adjustment of connected plate (C), finish of connected plate assembly (D).

#### 4. Results and Discussion

The results of the tensile experiments are shown in Table 4. The cylinder samples were fractured at about 1069.6 MPa, weaker than 1340 MPa, which is the normal value of the tensile strength of IN718 parts manufactured by casting. This may be because of the micro-segregation of IN718 during processing.

**Table 4.** Results of tensile tests.

Material	Process	Yield Strength/MPa	Tensile Strength/MPa	Elongation	
IN718	cast	1100	1340	12%	
	SLM	X-Y	780	1069.6	30.9%
		Z	634	980	-

The results of the compression tests are shown in Figure 26. The samples of 0.5 mm and 1.0 mm diameter were compressed perpendicularly while the sample of 1.5 mm occurred with lateral

compression. The samples of 2.0 mm and 2.5 mm were not fractured because of the limitation of the test machine.

The compression curves were recorded in Figure 27. At the beginning of the experiment the deformation of samples was elastic. Some support cylinders of the 0.5 mm sample yielded when the load increased to 180 MPa because of the local defects caused by the SLM process. At the same time, the modulus of elasticity of the parts decreased and the elastic deformation continued to occur. All the support cylinders yielded when the load increased to 338 MPa. The defects created by the SLM process may weaken the performance of parts, especially when the size of the structure is rather small.

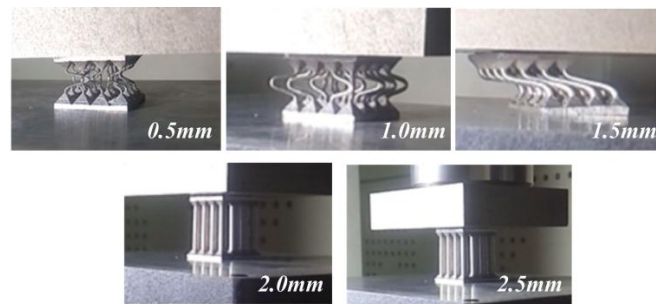


**Figure 26.** Results of compression tests.

Elastic deformation also occurred in the compression test of the 1.0 mm and 1.5 mm samples. When the displacement exceeded 0.75 mm, these parts yielded. Because of the limitation of the equipment, only a portion of the compression curves of the 2.0 mm and 2.5 mm samples were recorded.

The equivalent elastic modulus and yield stress can be calculated by the compression curves. The calculation results are shown in Table 5. It can be seen from Table 5 that the performance degradation of the parts becomes significant when the size of the structure is small. The mechanical properties of the small-size lattice structure might be poor due to the high aspect ratio of the rods. Higher aspect ratios increase the tendency of the structure to buckle, leading to poor mechanical properties.

**Table 5.** Calculation results of compression tests.

Number	Equivalent Diameter/mm	Yield Stress/MPa	Equivalent Stiffness/GPa
0.5 mm	2	180 (First) 338 (second)	49.03
1.0 mm	4	620.2	63.85
1.5 mm	6	694	57.33
2.0 mm	8		35.60
2.5 mm	10		30.45

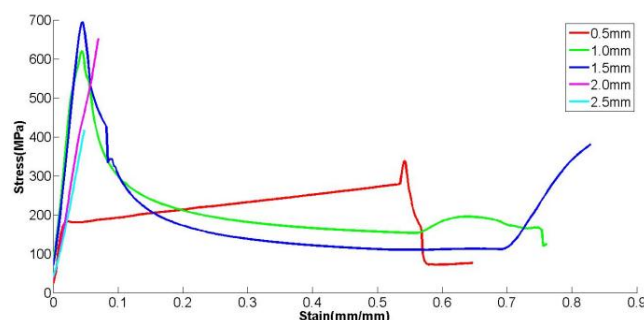


**Figure 27.** Compression curves of different sized samples.

The yield stress increases with the increase of the structure size. When the sizes were between 1.0 and 1.5 mm, the structure gradually returned to normal yield strength levels of the material. Thus, when the minimum structure size is more than 1.5 mm, the mechanical characteristics will almost not be affected by the defects brought by the SLM process.

The redesigned stopper and connecting plate were manufactured by the SLM process and the results are shown in Figure 28. The mass of the original stopper is 795.2 g and that of the redesigned one is 580.0 g with a weight reduction of about 27%. At the same time, the mass of the solid connecting plate is 3733.6 g. The weight decreased to 2150.9 g with a weight reduction of about 42.4% after the redesign of the inner structures.

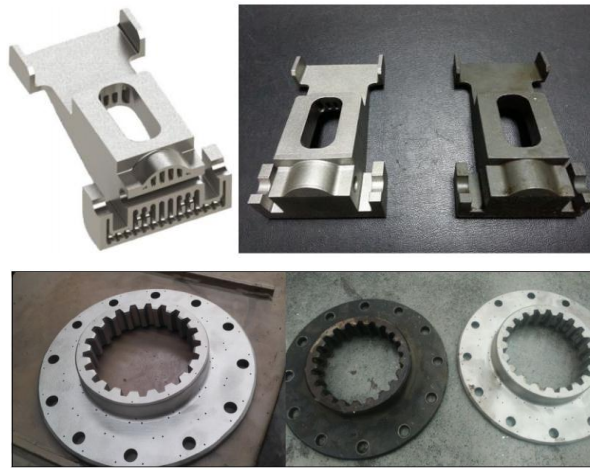


**Figure 28.** Final redesigned stopper (**up**) and connecting plate (**down**) with original parts.

Besides, after the application test shown in Figure 25, the connecting plate was taken out to check for damage. There are only slight wear marks on the tooth surface, and other parts of the structure were still in good condition. According to these tests we can conclude that the proposed lightweight structure redesign method can decrease the weight and cost of parts. Besides, the redesigned components have good mechanical characteristics and can meet the requirements of use.

## 5. Conclusions

In this paper, the tensile tests of parts manufactured by the SLM process were performed to study the characteristics of SLM components. The samples were fractured at about 1069.6 MPa in tensile tests, weaker than 1340 MPa, which is the normal value of the tensile strength of IN718 parts manufactured by casting. This maybe because of the micro-segregation of IN718 during SLM processing. A group of standard parts which have lattice structures with different sizes were manufactured by SLM. The mechanical tests of these candidates were also performed to study the trends of the yield process of different structure sizes. The compression testing results show that when the minimum structure size is larger than 1.5 mm, the mechanical characteristics will hardly be affected by process defects.

This paper investigated a new design method of lightweight parts manufactured by selective laser melting (SLM) based on the “Skin-Frame”. This method disassembled parts by their shapes and force conditions and reconstructed the inner structures of each divided one by the corresponding framework structures which were optimized by the finite element method. Then, we mixed them together by their topological relationship. Optimized foundation frameworks can be reserved to build a framework library, which can greatly shorten the design time using this method. The design of new parts can be as easy as selecting fundamental frameworks to fill the parts, though, of course, it requires substantial time to build this library. The stopper and connecting plate were redesigned by this method, with weight decreases of about 27% and 42.4%, respectively. Besides, the connecting

plate was tested in an armored vehicle in various conditions. The results show that the redesigned components can meet the requirements of use and decrease the cost and weight of parts.

The findings in this paper provide a foundation for lightweight part design. This research illustrates that parts manufactured by the SLM process with a small size are more vulnerable to process defects. This redesign method has been applied in some automobile parts such as the stopper and connecting plate. The cost and manufacture time of SLM parts can be cut down with this method. This method is a complement to current lightweight design methods. It can also be widely used in the fields of the automotive industry, aviation industry, spacecraft and so on.

This design method only focused on some common parts such as the stopper and connecting plate. Thus, the universality of the method was limited by the component types analyzed before. The mechanical properties of the lattice structure in the compression tests might be poor due to the high aspect ratio of the rods. Further study should improve the universality of this method. Smaller-aspect-ratio samples will be fabricated and tested to eliminate this confusion in future research.

**Acknowledgments:** The authors would like to thank Qingbiao Zhang for the preparation of 3D printed specimens by the SLM process.

**Author Contributions:** Li Tang and Chunbing Wu conceived and designed the experiments; Chunbing Wu performed the experiments; Li Tang, Chunbing Wu and Zhixiong Zhang analyzed the data; Jianzhong Shang and Chao Yan wrote the paper.

**Conflicts of Interest:** The authors declare no conflict of interest.

## Nomenclature

$D_1$	location diameter of mounting hole
$D_2$	diameter of inner ring
$L$	fracture length
$L_0$	initial length
$N$	number of mounting hole
$P$	maximum load
$S$	section area
$\gamma$	thickness of dowel bar
$\sigma$	section stress
$\varepsilon$	elongation percentage
$\eta$	thickness of frame

## References

1. Kruth, J.P.; Froyen, L.; Vaerenbergh, J.V.; Mercelis, P.; Rombouts, M.; Lauwers, B. Selective laser melting of iron-based powder. *J. Mater. Process. Technol.* **2004**, *149*, 616–622. [[CrossRef](#)]
2. Parthasarathy, J.; Starly, B.; Raman, S.; Christensen, A. Mechanical evaluation of porous titanium (Ti6Al4V) structures with electron beam melting (EBM). *J. Mech. Behav. Biomed. Mater.* **2010**, *3*, 249–259. [[CrossRef](#)] [[PubMed](#)]
3. Harrysson, O.L.A.; Cansizoglu, O.; Marcellin-Little, D.J.; Cormier, D.R.; West, H.A. Direct metal fabrication of titanium implants with tailored materials and mechanical properties using electron beam melting technology. *Mater. Sci. Eng. C* **2008**, *28*, 366–373. [[CrossRef](#)]
4. Evans, A.G.; Hutchinson, J.W.; Fleck, N.A.; Ashby, M.F.; Wadley, H.N.G. The topological design of multifunctional cellular metals. *Prog. Mater. Sci.* **2001**, *46*, 309–327. [[CrossRef](#)]
5. Cansizoglu, O.; Harrysson, O.; Cormier, D.; West, H.; Mahale, T. Properties of Ti–6Al–4V non-stochastic lattice structures fabricated via electron beam melting. *Mater. Sci. Eng. A* **2008**, *492*, 468–474. [[CrossRef](#)]
6. Campanelli, S.L.; Contuzzi, N.; Ludovico, A.D.; Caiazzo, F.; Cardaropoli, F.; Sergi, V. Manufacturing and Characterization of Ti6Al4V Lattice Components Manufactured by Selective Laser Melting. *Materials* **2014**, *7*, 4803–4822. [[CrossRef](#)]

7. Wang, D.; Yang, Y.; Liu, R.; Xiao, D.; Sun, J. Study on the designing rules and processability of porous based on selective laser melting. *J. Mater. Process. Technol.* **2013**, *213*, 1734–1742. [[CrossRef](#)]
8. Hernandez-Nava, E.; Smith, C.J.; Derguti, F.; Tammam-Williams, S.; Leonard, F.; Withers, P.J.; Todd, I.; Goodall, R. The effect of defects on the mechanical response of Ti-6Al-4V cubic lattice structures fabricated by electron beam melting. *Acta Mater.* **2016**, *108*, 279–292. [[CrossRef](#)]
9. Mahshid, R.; Hansen, H.N.; Hojbjerg, K.L. Strength analysis and modeling of cellular lattice structures manufactured using selective laser melting for tooling applications. *Mater. Des.* **2016**, *104*, 276–283. [[CrossRef](#)]
10. Sing, S.L.; Yeong, W.Y.; Wiria, F.E.; Tay, B.Y. Characterization of Titanium Lattice Structures Fabricated by Selective Laser Melting Using an Adapted Compressive Test Method. *Exp. Mech.* **2016**, *56*, 735–748. [[CrossRef](#)]
11. Brandt, M.; Sun, S.J.; Leary, M.; Feih, S.; Elambasseril, J.; Liu, Q.C. High-Value SLM Aerospace Components: From Design to Manufacture. *Adv. Mater. Res.* **2013**, *633*, 135–147. [[CrossRef](#)]
12. Xiao, D.; Yang, Y.; Su, X.; Wang, D.; Luo, Z. Topology Optimization of Microstructure and Selective Laser Melting fabrication for Metallic Biomaterial Scaffolds. *Trans. Nonferr. Met. Soc. China* **2012**, *22*, 2554–2561. [[CrossRef](#)]



© 2016 by the authors; licensee MDPI, Basel, Switzerland. This article is an open access article distributed under the terms and conditions of the Creative Commons Attribution (CC-BY) license (<http://creativecommons.org/licenses/by/4.0/>).